THE JOURNAL OF PHYSICAL CHEMISTRY C

ARTICLE

pubs.acs.org/JPCC

First-Principles Modeling of the "Clean-Up" of Native Oxides during Atomic Layer Deposition onto III−V Substrates

Sylwia Klejna* and Simon D. Elliott

Tyndall National Institute, University College Cork, Dyke Parade, Cork, Ireland

ABSTRACT: The use of III−V materials as the channel in future transistor devices is dependent on removing the deleterious native oxides from their surface before deposition of a gate dielectric. Trimethylaluminium has been found to achieve in situ "clean-up" of the oxides of GaAs and InGaAs before atomic layer deposition (ALD) of alumina. Here we propose seven reaction mechanisms for "clean-up", featuring exchange of ligands between surface atoms, reduction of arsenic oxide by methyl groups, and desorption of various products. We use first-principles density functional theory (DFT) to determine which mechanistic path is thermodynamically favored. We also discuss the statistical likelihood of the interdependent pathways. "Clean-up" of an oxide film is shown to strongly depend on electropositivity of the precursor metal, affinity of the precursor ligand to the oxide, and the redox character of the oxide. The predominant pathway for a metalloid oxide such as arsenic oxide is reduction, producing volatile molecules or gettering oxygen from less reducible oxides. We therefore predict that "clean-up" of III−V native oxides mostly produces As_4 gas, but also GaAs solid or InAs solid. Most C is predicted to form C_2H_6 but with some C_2H_4, CH_4, and H_2O. An alternative pathway is nonredox ligand exchange, which is a pathway that allow nonreducible oxides to be cleaned up.

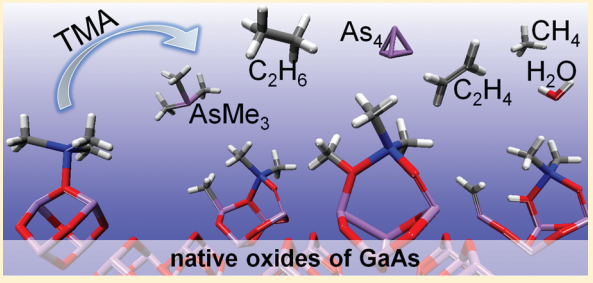

1. INTRODUCTION

As electronic devices are scaled down into the nanometer regime, their performance comes to depend on material interfaces, and even on individual layers of atoms. An example is the interface formed between high-permittivity (high-*k*) gate dielectric and semiconductor channel, which has been shown to be critical for the quality of metal oxide semiconductor (MOS) capacitors and transistors. The early stages of growth of the high-*k* dielectric films onto the semiconductor determine the interface properties, and therefore careful optimization of deposition conditions helps with improving device performance. Such a scalable film deposition technique, which allows growth of the high-*k* layers on high-mobility semiconductor substrates such as GaAs or other III−Vs, is atomic layer deposition (ALD).[1]

Although III−V/high-*k*-based devices have the potential to replace Si/SiO_2-based devices, a key issue is the lack of stable passivation of the interface. The high density of interface states is a cause of the Fermi-level pinning in the GaAs-based interface and is a source of slow traps, decreasing the efficiency of device operation.[2−5] Finding appropriate, stable passivation of the native oxides has been a puzzle for decades. Several methods have been used to increase the control over interfacial oxides between the dielectric and GaAs or $In_{0.53}Ga_{0.47}As$. It was shown that surface preparations, like cleaning (acids,[6,7] NH_4OH[8,9]), passivation (H_2S, $(NH_4)_2S$[7]), thermal treatment,[6] and forming a Si−interfacial passivation layer,[9] before high-*k* growth can reduce the density of interface traps (D_{it}). In particular many groups have reported a "clean-up" effect[8−13] by which the organometallic precursors trimethylaluminium (TMA or $AlMe_3$, where Me = CH_3) or tetrakis(ethylmethylamido)hafnium (TEMA−Hf or $Hf(NEtMe)_4$, where Et = C_2H_5) effectively reduce As and Ga oxides covering GaAs and InGaAs substrates and reduce D_{it}.[7,8,10,11,13] Although removing native oxides is not sufficient to solve the Fermi-level pinning problem,[14,15] it is an important step in the preparation of abrupt interfaces. This indicates that interfacial states can be controlled by optimizing the precursor exposure during the initial cycles of ALD deposition. This phenomenon was confirmed in many experiments, but detailed understanding of the chemistry of the reduction process is still missing.

It is commonly stated that the mechanism responsible for the "clean-up" effect is oxidation-state-dependent, as well as precursor-dependent, suggesting a ligand exchange mechanism.[8,11] Hinkle et al. suggest in their in situ analysis of ALD Al_2O_3 and HfO_2 deposition on GaAs surfaces that TMA removes As^{3+}, consistent with the Al^{3+} oxidation state in Al_2O_3, while TEMA−Hf is more likely to remove higher oxidation states (As^{5+}, Ga^{5+}, Ga^{4+}), since Hf is in the 4+ oxidation state in HfO_2. On the other hand there are studies showing that the reaction mechanism of "clean-up" appears to be nonselective toward reducing different As oxides.[13,16] This discrepancy might be due to different surface preparations and thermal treatments, and resultant differences in the chemistry of native oxides. Scanning transmission electron microscopy (STEM) shows a 20−25 Å thick Ga-rich oxide layer on gallium arsenide,[6] 10 Å thick after heating at 320 °C,[13] with increased

Received: July 11, 2011
Revised: November 3, 2011
Published: November 22, 2011

As concentration near the GaAs surface. There is the possibility of thermal conversion of As_2O_5 into As_2O_3 in the low pressure of the ALD chamber, with excess O_2 given off as a byproduct.[13,17] There may also be thermal conversion of mixed Ga/As oxide into predominantly Ga_2O_3.[13] Indeed, if the Ga−O bond is stronger than As−O, then this may explain why AsO_x loses oxygen more easily than GaO_x in "clean-up" with TMA. The experimental fact is that the initial TMA pulse (without a pulse of oxygen source) results in the formation of AlO_x, where the oxygen is presumably scavenged from AsO_x or GaO_x present on the substrate.[14,16]

In contrast with these observations there is no agreement in the literature about interfacial self-cleaning using chloride precursors ($HfCl_4$ or $TiCl_4$). "Clean-up" with the use of $HfCl_4$ as the metal precursor was not reported by Frank et al.[6] but was showed by Delabie et al.[18] Granados-Alpizar and Muscat show differences in surface reactions during GaAs exposure to TMA and $TiCl_4$ pulses.[16] It is demonstrated that both precursors remove the native oxide layer, but the mechanisms underlying this process seem to be fundamentally different. TMA deposits an Al_2O_3 layer and removes a portion of As from the surface, whereas $TiCl_4$ removes O and leaves the surface passivated with Cl atoms. The mechanism for removing oxides with the use of $HfCl_4$ differs also from the one for $TiCl_4$. It seems that growth of hafnium oxide is enhanced[18] and growth of titanium oxide is inhibited.[16] This diversity of precursor reactivity during the initial cycles of deposition cannot only be accounted for by the OH concentration on the native oxide surface. The surface chemistry of TMA on OH-terminated oxide is dominated by the mechanism where CH_4 is produced by transferring surface H to the methyl group of TMA.[19] Once protons are consumed in this way, there has to be another mechanism to account for removal of the native oxide.

The aim of this study is to find the mechanism responsible for "clean-up", i.e., for reduction or removal of As−O bonds on an oxidized GaAs substrate in the very first pulse of TMA during ALD of Al_2O_3. In particular we focus on the role of TMA as an agent to clean off the arsenic(III) oxide. We seek quantitative information on the energetics (ΔE), thermodynamics of the process (ΔG), and structures of intermediates and byproduct so that these can then be searched for experimentally. Specifically, we use plane wave density functional theory (DFT) to compute energetics of the reaction pathways leading to products that match experiment. We investigate several different reactions 1−7 with different sets of volatile products of As, C, and H, as no remnant products containing these elements were detected at the GaAs/AlO_x interface.[8,12]

$$\frac{1}{2}As_2O_3 + AlMe_3 \rightarrow \frac{1}{2}Al_2O_3 + AsMe_3 \quad (1)$$

$$\frac{1}{2}As_2O_3 + AlMe_3 \rightarrow \frac{1}{2}Al_2O_3 + \frac{1}{4}As_4 + \frac{3}{2}C_2H_6 \quad (2)$$

$$As_2O_3 + AlMe_3 \rightarrow \frac{1}{2}Al_2O_3 + \frac{1}{2}As_4 + \frac{3}{2}OMe_2 \quad (3)$$

$$\frac{1}{2}As_2O_3 + AlMe_3 \rightarrow \frac{1}{2}Al_2O_3 + AsH_3 + \frac{3}{2}C_2H_4 \quad (4)$$

$$\frac{1}{2}As_2O_3 + AlMe_3 \rightarrow \frac{1}{2}Al_2O_3 + \frac{1}{4}As_4 + \frac{3}{4}C_2H_4 + \frac{3}{2}CH_4 \quad (5)$$

$$As_2O_3 + AlMe_3 \rightarrow \frac{1}{2}Al_2O_3 + \frac{1}{2}As_4 + \frac{3}{2}C_2H_4 + \frac{3}{2}H_2O \quad (6)$$

$$4As_2O_3 + AlMe_3 \rightarrow \frac{1}{2}Al_2O_3 + 2As_4 + 3CO_2 + \frac{9}{2}H_2O \quad (7)$$

2. COMPUTATIONAL METHOD

First-principles DFT within the generalized gradient approximation (GGA) of Perdew and Wang (PW91)[20] for the exchange-correlation energy was applied as a reliable method for computation of the ground-state electronic structure and total energy. Using the VASP package,[21,22] 3-D periodic boundary conditions were imposed for a proper description of properties of crystalline materials. The core electrons were described with ultrasoft pseudopotentials (USPP)[23,24] projected into real space, and valence electrons were described with a plane wave basis up to a cutoff of 396 eV (except where otherwise noted). Geometry optimization was carried out with a sparse Monkhorst−Pack k-point sampling of reciprocal space, a medium/high FFT grid for surface/bulk (surf/b) calculations, respectively, and forces were converged to less than 10^{-3} eV $Å^{-1}$. Starting structures for optimization were generated "by hand" in a plausible sequence for the reactions of interest and were allowed to fully relax with no symmetry restraints.

To investigate the "clean-up" effect at a typical temperature of the ALD process, we neglect the constant contribution to entropy (S) from solid surfaces with adsorbates and have computed only the entropies of gaseous (g) species as ideal gases from $S = R \ln q$ where R is the gas constant and $q = q_t q_r q_v$ is a molecular partition function factorized into contributions from each mode of motion of the molecule (t, translational; r, rotational; v, vibrational), which are in turn obtained from vibrational analysis. The vibrational analysis was performed with the TURBOMOLE suite of quantum chemical programs[25] using DFT within the GGA parametrization by Perdew−Burke−Ernzerhof (PBE),[26] the resolution-of-the-identity (RI) approximation,[27,28] and atom-centered triple-ζ valence basis functions, augmented by double-polarization functions, TZVPP2.[29] Gibbs free energies (ΔG) could then be calculated from

$$\Delta G = \Delta E + \Delta ZPE - \Delta E^{vib} - T\Delta S \quad \text{(equation 1)}$$

where we consider only the contributions of the gaseous species to the zero-point energy term, ΔZPE, and to the vibrational energy term, $\Delta E^{vib}(T)$.

3. RESULTS

We take two approaches to modeling the candidate "clean-up" reactions 1−7. In the first approach we model crystalline oxides and isolated gas-phase molecules and thus determine the "bulk" thermodynamics of the reactions (section 3.1). In the second approach, we consider the explicit steps that occur as the TMA molecule reacts with a surface covered with arsenic oxide. The reaction is divided into three parts: TMA adsorption (section 3.3), methyl transfer (section 3.4), and desorption of volatile products (section 3.6). Our notation is to use arabic numerals for overall reactions, including the candidates for "clean-up". Lower-case letters and arabic numerals correspond to the intermediate "clean-up" reactions, e.g., 2a, 2b, etc., are intermediates for reaction 2. Surface models for adsorption, methyl transfer, and models for

Table 1. Computed Geometrical Parameters for the As_2O_3 Bulk and Its (010) Oriented Slab within a Cell Fixed at the Experimental Lattice Parameters[a]

geometry parameters	bulk	bulk (experiment)[b]	slab (010)
R(As−O)	1.823 Å	1.786(3) Å	1.819 Å
∠(As−O−As)	127.5°	128.7(3)°	126.6°
∠(O−As−O)	99.1°	98.4°	99.8°

[a] For the slab structure, given values are an average for the entire supercell. [b] Ref 33.

surfaces after desorption of gaseous molecules are labeled with upper-case letters **A**−**Z**.

3.1. Bulk Potential Energies. To have a first overview on the energetics of "clean-up" reactions 1−7 we have used DFT to compute the potential energy at zero temperature $\Delta E_{(b)}$ and the thermodynamic Gibbs free energy at various temperatures $\Delta G_{(b)}$ for bulk structures in each reaction. High accuracy was used for all bulk calculations (α-Al_2O_3, α-As, α-As_2O_5, zinc blende-GaAs, β-Ga_2O_3, zinc blende-InAs, In_2O_3): convergence of energies to 10^{-3} eV with respect to coordinates of ions and cells, 130% of the standard plane wave cutoff energy, convergence with respect to k-point sampling. The total energy versus volume for all models of the bulk structures was optimized resulting in equilibrium lattice parameters that agreed well with experiment (with deviation less than 2%).[30]

A special case was the model for arsenic(III) oxide since its crystalline structure did not allow us to perform cell shape optimization within DFT. This crystalline form, known as arsenolite, is the polymorph of solid arsenic(III) oxide that has been reported to grow as a result of oxidation of the GaAs surface[31,32] and, therefore, was chosen here as a model for the oxidized III−V substrate. Arsenolite is a molecular solid built of a cubic tetrahedral array of As_4O_6 molecules with rings of four connected pyramidal AsO_3 units that share O atoms.[33,34] The intermolecular interaction is of the van der Waals type. Present DFT methods are not able to completely describe this type of weak interaction,[35,36] and therefore experimental lattice constants had to be used for the As_2O_3 bulk model.[33] We are confident that this has no adverse effect on the reactions studied here as we draw no conclusions about the actual structure of As_2O_3 or Al_2O_3 layers. Ions were fully relaxed within the fixed As_2O_3 cell, and the calculated geometry parameters compare well with the experimental values, with the deviation around 2%, in line with other theoretical results[37,38] (see Table 1).

Geometry optimization for gas species ($AlMe_3$, $AsMe_3$, AsH_3, As_4, CH_4, C_2H_4, C_2H_6, CO_2, $GaMe_3$, H_2O, $InMe_3$, OMe_2) was also performed with the plane wave periodic code using a big simulation box, cubic or rhombohedral, with a = 15 Å lattice constant, ensuring enough space for the gas molecule to be effectively surrounded by vacuum and unhindered by its periodic images. Six k-points were located at the edges of the first Brillouin zone. However, as outlined in the previous section, ΔS was computed via vibrational analysis using a nonperiodic code.

Table 2 and Figure 1 show the computed change in energy at 573 K ($\Delta G_{(b)}^{573K}$) and at 0 K ($\Delta E_{(b)}^{0K}$) for proposed "clean-up" reactions 1−7. Figure 1 shows also the temperature dependence over the range of 0−1200 K of the free energy for reactions 1−7.

The most favorable reaction at all temperatures of interest is reaction 7. The complete oxidation process of methyl groups to carbon dioxide is strongly exothermic and requires the transfer of 24 electrons per TMA reacting. Four formula units of arsenic oxide are reduced to gaseous elemental arsenic in this reaction. Water is also produced giving −15.7 eV/TMA at a typical ALD process temperature.

Reactions 1−6 are thermodynamically competitive with one another at ALD deposition temperatures. Reactions 2, 3, 5 and 6 are thermodynamically approximately equal, releasing −5.6, −4.6, −5.8, −6.3 eV/TMA, respectively, at 573 K. These reactions involve reduction of arsenic(III) to elemental As in the form of gaseous As_4 and oxidation of methyl groups to ethane (C_2H_6) in reaction 2, dimethyl ether (OMe_2) in reaction 3 or ethene (C_2H_4), the latter with the formation of methane (CH_4) in reaction 5 or water in reaction 6. An alternative possible reaction at low temperature is nonredox ligand transfer (reaction 1), where each reacting TMA molecule produces volatile trimethylarsenic ($AsMe_3$), still arsenic(III), and energy −4.0 and −4.4 eV at 573 and 0 K, respectively. The least possible mechanism with the change in energy −3.6 or −2.3 eV/TMA at 573 or 0 K, respectively, is reduction of As^{3+} to molecular arsine (AsH_3) and oxidation of methyl groups to molecular ethene (C_2H_4) (reaction 4).

All of these except reaction 1 involve reduction of As and oxidation of C. The number of electrons transferred is 0, reaction 1, 3, reactions 2 and 5, 6, reactions 3, 4 and 6, and 24, reaction 7 per TMA reacting. In all cases, O^{2-} is transferred from arsenic to aluminum(III), presumably driven by the strength of Al−O bonding. However, note that the oxidation states of O and Al do not change.

The bulk energetics can be used to investigate some side reactions of the products. We find that disproportionation of As_4 under the action of CH_4 is not favored at any temperatures (Figure 2):

$$\frac{1}{2}As_4(g) + 3CH_4(g) \rightarrow AsMe_3(g) + AsH_3(g), \quad \Delta G_{(b)}^{573K} = +3.9\ \text{eV} \tag{8}$$

Decomposition of dimethyl ether to ethane and water is favored at all temperatures:

$$\frac{3}{2}OMe_2(g) \rightarrow \frac{3}{2}C_2H_4(g) + \frac{3}{2}H_2O(g), \quad \Delta G_{(b)}^{573K} = -1.6\ \text{eV} \tag{9}$$

C_2H_4 and CH_4 are computed to be slightly more favorable products at the ALD process temperature than C_2H_6:

$$\frac{3}{2}C_2H_6(g) \rightarrow \frac{3}{4}C_2H_4(g) + \frac{3}{2}CH_4(g), \quad \Delta G_{(b)}^{573K} = -0.2\ \text{eV} \tag{10}$$

This explains why reactions 2 and 5 are thermodynamically the same, with C_2H_4 and CH_4 formation slightly more favorable at higher temperatures (above 500 K).

Disproportionation of C_2H_6 and C_2H_4 under the action of H_2O is favored:

$$\frac{3}{2}C_2H_6(g) + \frac{3}{4}H_2O(g) \rightarrow \frac{3}{8}CO_2(g) + \frac{21}{8}CH_4(g), \quad \Delta G_{(b)}^{573K} = -1.0\ \text{eV} \tag{11}$$

dx.doi.org/10.1021/jp206566y |J. Phys. Chem. C 2012, 116, 643–654

Table 2. Gibbs Free Energies at 573 K ($\Delta G_{(b)}^{573K}$) and Energies at 0 K ($\Delta E_{(b)}^{0K}$) for Possible Products of "Clean-up" Reaction of As_2O_3[a]

reaction		$\Delta G_{(b)}^{573K}$	$\Delta E_{(b)}^{0K}$
$\frac{1}{2}As_2O_3 + AlMe_3 \rightarrow \frac{1}{2}Al_2O_3 + AsMe_3$	(1)	−4.0	−4.4
$\frac{1}{2}As_2O_3 + AlMe_3 \rightarrow \frac{1}{2}Al_2O_3 + \frac{1}{4}As_4 + \frac{3}{2}C_2H_6$	(2)	−5.6	−5.2
$As_2O_3 + AlMe_3 \rightarrow \frac{1}{2}Al_2O_3 + \frac{1}{2}As_4 + \frac{3}{2}OMe_2$	(3)	−4.6	−3.2
$\frac{1}{2}As_2O_3 + AlMe_3 \rightarrow \frac{1}{2}Al_2O_3 + AsH_3 + \frac{3}{2}C_2H_4$	(4)	−3.6	−2.3
$\frac{1}{2}As_2O_3 + AlMe_3 \rightarrow \frac{1}{2}Al_2O_3 + \frac{1}{4}As_4 + \frac{3}{4}C_2H_4 + \frac{3}{2}CH_4$	(5)	−5.8	−4.5
$As_2O_3 + AlMe_3 \rightarrow \frac{1}{2}Al_2O_3 + \frac{1}{2}As_4 + \frac{3}{2}C_2H_4 + \frac{3}{2}H_2O$	(6)	−6.3	−3.1
$4As_2O_3 + AlMe_3 \rightarrow \frac{1}{2}Al_2O_3 + 2As_4 + 3CO_2 + \frac{9}{2}H_2O$	(7)	−15.7	−2.5

[a] Given energies are bulk potential energies. All energies are shown in eV per $AlMe_3$ molecule reacting with arsenic(III) oxide.

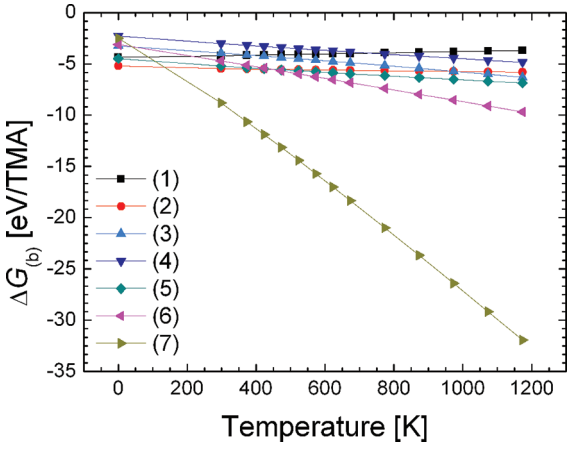

Figure 1. Temperature dependence of free energy for "clean-up" reactions applied to bulk solids and gas-phase molecules 1−7.

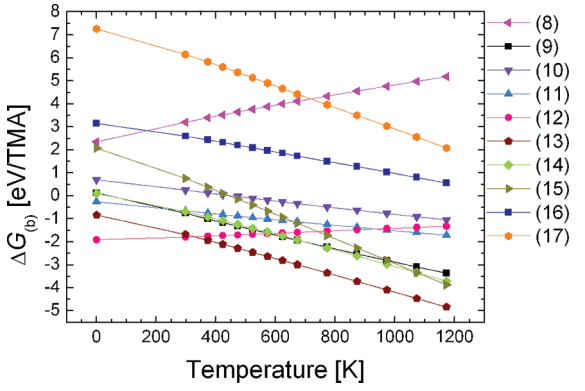

Figure 2. Temperature dependence of free energy for side reactions of the gas products 8−12 and alternative "clean-up" reactions 13−17.

$$\frac{3}{2}C_2H_4(g) + \frac{3}{2}H_2O(g) \rightarrow \frac{3}{4}CO_2(g) + \frac{9}{4}CH_4(g),$$
$$\Delta G_{(b)}^{573K} = -1.6\ eV \quad (12)$$

Carbon oxidation to its highest oxidation state in CO_2 is a potentially exothermic reaction, depending on the source of the oxygen. Water is here relatively weak oxidizing agent. By comparing to reaction 7, which is strongly exothermic at any temperature higher than 0 K, we see that arsenic oxide is a strong oxidizing agent.

By combining with the original "clean-up" reactions, we can propose alternative surface treatments, not involving TMA, that will result in the same "clean-up" effect but without the formation of Al_2O_3:

$$\frac{1}{2}As_2O_3(b) + AsH_3(g) \rightarrow \frac{1}{2}As_4(g) + \frac{3}{2}H_2O(g),$$
$$\Delta G_{(b)}^{573K} = -2.6\ eV \quad (13)$$

$$\frac{1}{2}As_2O_3(b) + \frac{1}{4}C_2H_4(g) \rightarrow \frac{1}{4}As_4(g) + \frac{1}{2}CO_2(g) + \frac{1}{2}H_2O(g),$$
$$\Delta G_{(b)}^{573K} = -1.6\ eV \quad (14)$$

$$\frac{1}{2}As_2O_3(b) + \frac{3}{2}C_2H_6(g) \rightarrow \frac{1}{4}As_4(g) + \frac{3}{2}C_2H_4(g) + \frac{3}{2}H_2O(g),$$
$$\Delta G_{(b)}^{573K} = -0.7\ eV \quad (15)$$

The most promising of these is probably the proposal to use AsH_3. In fact, reports by Reinhardt et al.[39] showed that an oxidized GaAs (001) surface was deoxidized at around 350 °C (625 K), certainly at 400 °C under H_2 and AsH_3 constant flow. The annealing in AsH_3 prevents the decomposition of the GaAs and keeps it smooth during oxide desorption.[40−43] Our calculations add some extra information: this "deoxidation" may be reduction by AsH_3 according to reaction 13, rather than just decomposition of As_2O_3 into arsenic and oxygen (reaction 16). Thermal decomposition of As and Ga oxides occurs above 850 K and at very low vacuum as shown in refs 40−43 and computed

here for reactions

$$\frac{1}{2}As_2O_3(b) \rightarrow As(b) + \frac{3}{4}O_2(g), \quad \Delta G_{(b)}^{900K,\,10^{-20}atm} = -0.3\ eV \tag{16}$$

$$\frac{1}{2}Ga_2O_3(b) + \frac{1}{2}As_2O_3(b) \rightarrow GaAs(b) + \frac{3}{2}O_2(g), \quad \Delta G_{(b)}^{1000K,\,10^{-20}atm} = -0.3\ eV \tag{17}$$

This means that thermal removal of oxides can imitate the known clean-up effect under harsh conditions, but the same can be achieved under moderate conditions via reduction by arsine. However, none of these is more energetically favored than the original "clean-up" reactions at any temperature of interest (Figure 2).

3.2. As_2O_3 (010) Surface Structure. In more detailed calculations, we have looked at the mechanism of the reactions on model surfaces. A model of the As_2O_3 surface was built by cleaving the relaxed bulk structure at the low-index (010) plane between molecular units. The (010) plane is the natural cleavage direction which creates a surface free of dangling bonds. To verify stability of the (010) oriented surface, its formation energy (σ) as a function of slab thickness was tested for slabs up to 20 layers thick using[44]

$$\sigma = \lim_{N\rightarrow\infty}\frac{1}{2}(E_{slab}^{N} - NE_{bulk}) \qquad \text{(equation 2)}$$

where E_{slab}^{N} is the total energy of N-layer slab and E_{bulk} is the bulk total energy. As can be seen in Figure 3, the surface energy is determined to be 0 eV/Å^2 with an uncertainty below 1.5 meV/Å^2. This zero surface energy correlates well with the weak interaction between molecular units in the crystalline structure, although, as noted above, DFT-PW91 does not describe the interaction correctly. Similar results have been obtained by Ganduglia-Pirovano and Sauer for surface optimization of the molecular solid V_2O_5.[45]

The oxide substrate surface is modeled by periodic slabs separated by 10 Å of vacuum. We use a 1 × 2 supercell that contains one layer totalling four molecular units of As_4O_6 (40 atoms). For all slab calculations medium accuracy was used in VASP with plane wave cutoff of 396 eV and 2 × 1 × 1 k-point mesh.

3.3. TMA Adsorption onto the As_2O_3 Surface. TMA adsorbs onto oxide surfaces in an associative way, forming a Lewis adduct between Al and surface oxygen. The mechanism for this reaction is well-known and has been described in previous studies on other oxides.[19,46] For the (010) oriented arsenic oxide surface (**A**, Figure 4), overlap of the empty p orbital of Al atom in horizontal TMA with the lone pair of electrons on surface oxygen is easy and not hindered by geometry (**B**, Figure 4). The Al−O bond length is computed to be 2.0 Å, and the calculated adsorption energy is $\Delta E_{(surf)}^{0K} = -0.7$ eV (Table 3). This agrees very well with the same reaction on Al_2O_3.[19] The calculated Gibbs free energy, $\Delta G_{(surf)}^{573K} = +2.5$ eV (minimum B, Figure 8), is positive for adsorption, as expected. The adsorbate molecule loses translational motion, which is the main contribution to the entropy (see section 2). This means that it is not thermodynamically favored for TMA to adsorb molecularly but that subsequent TMA dissociation on the surface may lead to $\Delta G < 0$.

3.4. Methyl Transfer Mechanisms at the Surface. We have identified ligand transfer as the primary reaction of decomposition of chemisorbed $AlMe_3$ (**B**, Figure 4) on arsenic(III) oxide (**A**, Figure 4). Successive dissociation of Me from $AlMe_3$ leads to

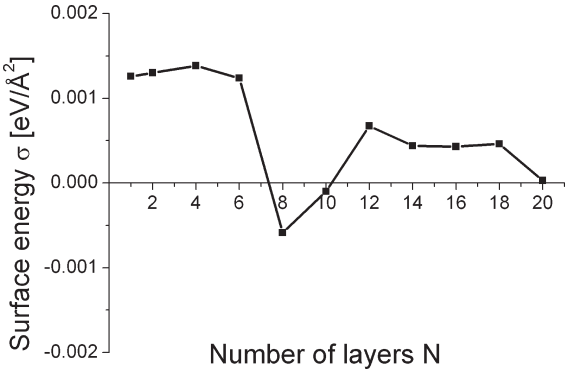

Figure 3. Surface formation energies (σ) for As_2O_3 (010) as a function of the slab thickness (number of layers N, where a layer is defined as a two molecular units of As_4O_6).

surface species of the type $(\|O-)_{1+n}AlMe_{3-n} + n\|X-Me$, where n = 1, 2, 3 is the number of Me groups transferred and $\|X$ is a binding site of the surface. Specifically, this dissociation can occur on surface As atoms and/or surface O atoms: X = As and/or O. On an oxidized III−V surface, one would also consider X = In, Ga, etc., but this is beyond the scope of the current paper. Computed energetics for the formation of these products are shown in Table 3 with the corresponding structures in Figure 4. Entropy changes are assumed to be negligible during methyl transfer on the surface with no adsorption or desorption, i.e., $\Delta G_{(surf)} = \Delta E_{(surf)}^{0K}$ at all temperatures.

According to our simulations the initial step of decomposition of $AlMe_3$ (n = 1) is splitting of Al−Me and binding of the methyl group to a surface arsenic atom: $\|As-Me$. Structure **E** is the lowest energy product that we found, where near-tetrahedral geometry for Al is preserved: Al is bound to two surface oxygen atoms and two remaining methyl groups, $(\|O-)_2AlMe_2$. The energy change for this reaction is computed to be −1.0 eV relative to **A** and −0.3 eV relative to **B** (Table 3). Therefore, we can propose a mechanism as follows:

$$\|O-Al(Me^-)_3 \rightarrow (\|O-)_{1+n}Al(Me^-)_{3-n} + n\|As-Me^- \quad (n = 1, 2, 3) \tag{18}$$

The other possibility of dissociation of $AlMe_3$ in this step is the one where the Me group binds to O ($\|O-Me$, **D**), which is computed to be slightly unfavorable ($\Delta E_{(surf)}^{0K} = 0.3$ eV relative to **B**). Transferring Me to O is expected to be accompanied by the transfer of electrons. The Me^- group on Al becomes oxidized to Me^+ on O, releasing two electrons. The general reaction for this mechanism can be written as

$$\|O-Al(Me^-)_3 \rightarrow (\|O-)_{1+n}Al(Me^-)_{3-n} + n\|O-Me^+ + 2ne^- \quad (n = 1, 2, 3) \tag{19}$$

The optimized structure (**D**) shows an As−As bond, suggesting that the electrons are transferred from carbon to arsenic (see section 3.5).

Proton diffusion according to the reaction: $\|As-Me \rightarrow \|As{=}CH_2 + H^+ + 2e^-$ is a further decomposition reaction that can contribute to the mechanism for reactions 4−6. The computed energy ($\Delta E_{(surf)}^{0K} = 0.3$ eV) suggests that there may be a high barrier for this reaction. The optimized structure is shown in Figure 4 labeled as **C**. On the other hand, further proton diffusion seems to be favorable, as in reaction **F**: $2\|As-Me \rightarrow 2\|As{=}CH_2$

dx.doi.org/10.1021/jp206566y |J. Phys. Chem. C 2012, 116, 643–654

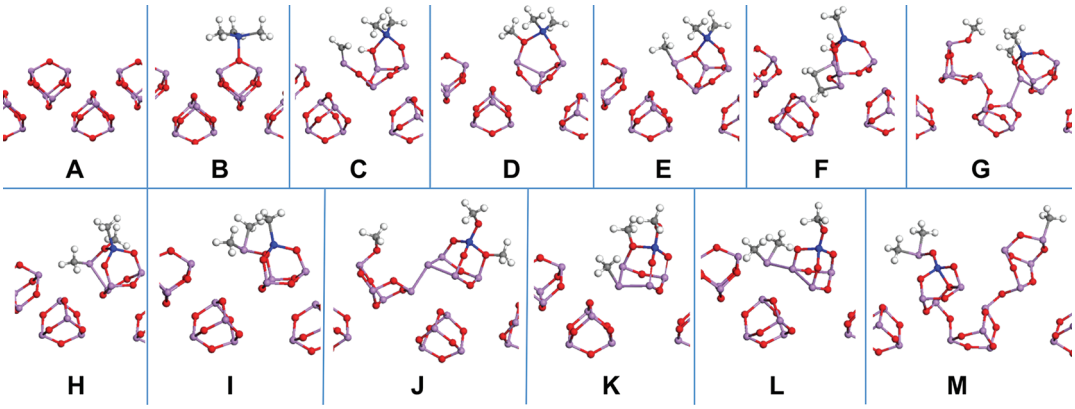

Figure 4. Surface models for adsorption of $AlMe_3$ onto the As_2O_3 surface (**A** and **B**) and Me group transfer (**C**−**M**) onto different atoms (surface O or surface As). Ball and stick representation: purple As, red O, blue Al, gray C, and white H.

Table 3. Reaction Energies ($\Delta G_{(surf)} = \Delta E^{0K}_{(surf)}$) for Adsorption of $AlMe_3$ onto As_2O_3 Surface (A and B) and Me Group Transfer (C−M) onto Different Surface Atoms (Surface O or Surface As), as Illustrated in Figure 4[a]

	products at surface	$\Delta E^{0K}_{(surf)}$
A	$4As_4O_6(surf) + AlMe_3(g)$	0.0
B	$\|\|O{-}AlMe_3$	−0.7
C	$(\|\|O{-})_2AlMe_2 + \|\|As{=}CH_2 + \|\|O{-}H + 2e^-$	+0.3
D	$(\|\|O{-})_2AlMe_2 + \|\|O{-}Me + 2e^-$	−0.4
E	$(\|\|O{-})_2AlMe_2 + \|\|As{-}Me$	−1.0
F	$(\|\|O{-})_3AlMe + 2\|\|As{=}CH_2 + 2\|\|O{-}H + 4e^-$	−0.3
G	$(\|\|O{-})_3AlMe + 2\|\|O{-}Me + 4e^-$	−0.4
H	$(\|\|O{-})_3AlMe + \|\|As{-}Me + \|\|O{-}Me + 2e^-$	−1.3
I	$(\|\|O{-})_3AlMe + 2\|\|As{-}Me$	−2.5
J	$(\|\|O{-})_4Al + 3\|\|O{-}Me + 6e^-$	−1.4
K	$(\|\|O{-})_4Al + \|\|As{-}Me + 2\|\|O{-}Me + 4e^-$	−1.7
L	$(\|\|O{-})_4Al + 2\|\|As{-}Me + \|\|O{-}Me + 2e^-$	−2.4
M	$(\|\|O{-})_4Al + 3\|\|As{-}Me$	−2.9

[a] Energies are in eV per $AlMe_3$ molecule reacting with As_2O_3 and relative to **A**.

$+ 2H^+ + 4e^-$ with $\Delta E^{0K}_{(surf)} = -0.3$ eV relative to **A**. The relaxed structure **F** shows that once two methylene groups ($=CH_2$) are formed, a C−C bond appears, but As−C is strong enough to keep it from desorption as C_2H_4 (Figure 4). In general we can write the reaction

$$\|O{-}Al(Me^-)_3 \rightarrow (\|O{-})_{1+n}Al(Me^-)_{3-n} + n\|As{=}CH_2 + n\|O{-}H^+ + 2ne^- \quad (n = 1,2,3) \qquad (20)$$

The second methyl group transfer ($n = 2$) gives a product of the type $(\|O{-})_3AlMe$, with the transferred group on O again ($2\|O{-}Me$, **G**), on both ($\|As{-}Me + \|O{-}Me$, **H**), or on As again ($\|As{-}Me_2$, **I**). We found that the formation of $\|As{-}Me_2$ (**I**) is the most energetically favorable, with a change in energy of −2.5 eV relative to **A**. Transferring a second Me to As is of the same type as described above for **E**, since Al and As are in the same formal oxidation state (+3). Formation of $\|As{-}Me + \|O{-}Me$ (**H**) gives only −1.3 eV (see Table 3) and requires oxidation of one Me group, similar to **D**. The least plausible is oxidation of two Me groups in **G** with a change in energy of only −0.4 eV relative to **A**, isoenergetic with **D**. It is therefore likely that the

Table 4. Differences in Bader Atomic Charges (ΔQ) between Selected Atoms from Structures B, D, and E (Figure 4)[a]

atom	ΔQ(B → E)	ΔQ(E → D)
As	0.0	0.0
As^1	0.1	1.1
As^2	0.0	1.0
C	0.1	0.1
C^1	0.2	−1.7

[a] Selected atoms are labeled on structures **D** and **E** (Figure 6).

D → **G** redox reaction is reversible. For all structures (**F**, **G**, **H**, **I**) Al is roughly tetrahedral, coordinated to three O sites and the last remaining Me group.

We find that dissociation of the final Me ($n = 3$) from Al leads to products of the type $(\|O{-})_4Al + 3\|X{-}Me$ with four O atoms bound to surf-Al. There are four possibilities for this reaction: all three Me on O atoms ($3\|O{-}Me$), one Me on As and two Me on O atoms ($\|As{-}Me + 2\|O{-}Me$), two Me on As atoms and one on O ($2\|As{-}Me + \|As{-}O$), or all three Me on As atoms ($3\|As{-}Me$). Structures **J**, **K**, **L**, and **M**, respectively, are the lowest energy structures that we have found for this dissociation (Figure 4). Again the energetically most probable scenario is dissociation of TMA onto arsenic atoms. This liberates $\Delta E^{0K}_{(surf)} = -2.9$ eV (**M**, Table 3). Relative to this, transfer of successive Me to O costs energy: **L** has $\Delta E^{0K}_{(surf)} = -2.4$ eV, **K** has $\Delta E_{(surf)}{}^{0K} = -1.7$ eV, and **J** has $\Delta E^{0K}_{(surf)} = -1.4$ eV. The redox reaction **I** → **L** is thus energetically nearly neutral and probably reversible. Oxidation of three methyl groups partially reduces four As atoms, and three covalent As−As bonds appear in the relaxed structure **J**.

Our computations thus reveal the overall trends in energetics of TMA decomposition onto arsenic or oxygen atoms. The energy liberated by breaking an Al−Me bond and forming As−Me ranges from −0.3 to −1.5 eV. On the other hand, forming an O−Me bond is less energetically favored, ranging from −0.2 to +0.3 eV, even if an As−Me bond is already present. What is more, oxidizing a Me group is strongly uphill when Me transfer occurs from As to O (ranges from 0 to +1.2 eV). This suggests that the As−C bond is strong. Bader population of the As−Me bond has shown no significant change in charges on atoms relative to Al−Me, suggesting that the formal oxidation state Me^- is preserved (see Table 4).

dx.doi.org/10.1021/jp206566y | J. Phys. Chem. C 2012, 116, 643–654

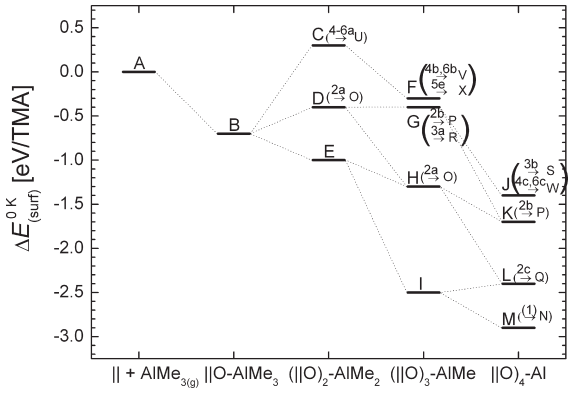

Figure 5. Potential energy surface ($\Delta G_{(surf)} = \Delta E^{0K}_{(surf)}$) showing the minima for structures **A**−**M** in the methyl transfer steps that form part of surface reactions 1−6 (Table 5) and give surface products **N**−**Z**, Figure 7, as typed-in brackets. The corresponding numerical values (in eV per $AlMe_3$ molecule reacting with As_2O_3 at 0 K) are shown in Table 3 with surface models shown in Figure 4.

3.5. Population Analysis of Reduced Structures. The Bader population analysis was carried out by using Transition State Tools (TST) for VASP developed at the University of Texas.[47−49] Table 4 shows the resulting differences in valence charges associated with selected atoms from structures **B**, **D**, and **E**. It is shown that during Me transfer onto As there is negligible reorganization in the electronic populations (see $\Delta Q(\mathbf{B} \rightarrow \mathbf{E})$ Table 4), which means that no charge transfer occurred. As mentioned before, transferring Me to O is expected to cause the transfer of electrons since, formally, oxidizing the Me^- group to Me^+ releases two electrons. This is confirmed in the difference between valence atomic charges of the carbon atom denoted C^1 (see Figure 6 for labels) that is bound with O or As in structures **D** or **E**, respectively. This $\Delta Q(\mathbf{E} \rightarrow \mathbf{D})$ for C^1 is determined to be $-1.7e$. Released electrons are accepted by As atoms, which is manifested in formation of the As^1−As^2 bond in structure **D** ($R(As^1-As^2)$ = 2.619 Å). ΔQ increases from 0.0e for "surface" arsenic As (formal oxidation state +3) to 1.1e and 1.0e for As^1 and As^2, respectively, so that the electron pair is shared in the newly formed As_2 dimer and formal oxidation state of these arsenic atoms would be +2.

3.6. Production of Various Volatile Species. As stated in section 3.4, decomposition of trimethylaluminum on arsenic oxide may lead to formation of multiple products on the surface. This may result in desorption of nine volatile species: As_4, $AsMe_3$, AsH_3, CH_4, C_2H_4, C_2H_6, CO_2, H_2O, and OMe_2 according to reactions 1−7. We have computed the temperature dependence of Gibbs free energies for these reactions at the surface ($\Delta G_{(surf)}$) which is shown in Figure 9. A schematic of the potential free energy surface at a typical ALD temperature is shown in Figure 8 with values in Table 5 and structures of products in Figure 7.

If there is sufficient concentration of ||As−Me groups on the surface (**M**, Figure 4), trimethylarsine may be formed from As^{3+} without any redox via reaction 1 to give product **N**, Figure 7. This process is exothermic: $\Delta G^{573K}_{(surf)} = -2.4$ eV per TMA (see Table 5 for energetics of surface reactions), but desorption of $AsMe_3$ is less favored than formation of surface products ||As−Me_n. The computed energies for reaction 1 are also much smaller compared to redox surface reactions 2, 5, and 6. As noted above, the energetics of ligand transfer on the surface favor Me transfer from Al to As. However, transfer to O, concomitant with partial reduction of surface As, will close off the possibility of desorption as As^{3+} in

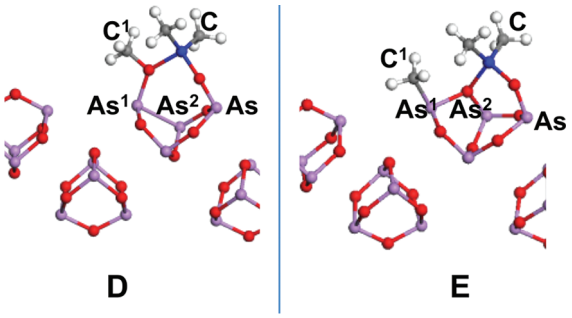

Figure 6. Structures **D** and **E** with atoms labeled for the Bader charge analysis in Table 4.

reaction 1. In this way, we see that each surface reaction affects the surface concentration of reactants for the other reactions.

As shown in previous sections, each decomposition of TMA on surface oxygen atoms causes a transfer of electrons and reduction of surface arsenic. Arsenic(III) oxide can be reduced to elemental arsenic or even to molecular arsine (formal −3 oxidation state) as shown in redox reactions 2−7. This requires transferring three or six electrons per arsenic atom accordingly:

$$As^{3+} + 3e^- \rightarrow As^0 \quad [(1/4)As_4] \tag{21}$$

or

$$As^{3+} + 6e^- \rightarrow As^{3-} \tag{22}$$

This shows that decomposition of multiple TMAs may lead gradually to the accumulation of charge on surface As and eventual desorption as AsH_3 or As_4, which is a possible volatile form of elemental As. Alternatively, reduced As may undergo other reactions (see section 4). The mechanism identified here of transferring electrons by Me transfer to surface O can produce up to six electrons per one TMA molecule (see reaction 19—transfer of three methyl groups to O gives six electrons). This approach allows us to evaluate surface energetics for production of an AsH_3 molecule or up to half of an As_4 molecule in reactions 2−6, which will be described below, but it does not allow us to evaluate the surface energy of reaction 7, where 24 electrons are transferred to produce two As_4 molecules. Modeling reaction 7 requires further consideration of proton diffusion, which was shown to be endothermic (**C**) and is beyond the scope of this paper. Nevertheless bulk energetics (section 3.1) showed this reaction to be the most exothermic "clean-up" reaction, where eight arsenics are reduced by one TMA and carbon is completely oxidized (from formally −4 in Me up to +4 in CO_2). One can only speculate that this kind of charge transfer is subject to kinetics, as will be discussed in the next section.

Our simulations show that formation of C_2H_6 in reaction 2 is spontaneous when Me groups in the right oxidation state, ||M−Me^- (M = Al, As) and ||O−Me^+, are close together. It can occur for most of the surface dissociation products studied in section 3.4 (when at least one Me group is oxidized: structures **D**, **G**, **H**, **K**, **L**, Figure 4), and so this is a statistically likely reaction. Desorption of the C_2H_6 molecule can lead to three types of products via reactions 2a, 2b, 2c: when the remaining Me group binds to Al, to O or to As, respectively, and the lowest energy structures that we have found are **O**, **P**, **Q**, respectively (see Figure 7). Again the most energetically favorable is a structure of the type ||As−Me with calculated energy for

dx.doi.org/10.1021/jp206566y |*J. Phys. Chem. C* 2012, 116, 643–654

Table 5. Reaction Gibbs Free Energies at 573 K ($\Delta G^{573K}_{(surf)}$) for Production of Volatile Species According to Reactions 1−6 and Their Intermediates Reactions 2a−6f[a]

surface reaction		surface product	gaseous product	$\Delta G^{573K}_{(surf)}$
(1)	**N**	$(\|\|O-)_4Al$	+ $AsMe_3$	−2.4
2a	**O**	$(\|\|O-)_3AlMe + 2e^-$	+ C_2H_6	−0.7
2b	**P**	$(\|\|O-)_4Al + \|\|O-Me + 4e^-$	+ C_2H_6	−0.9
2c	**Q**	$(\|\|O-)_4Al + \|\|As-Me + 2e^-$	+ C_2H_6	−1.6
(2)	**N**	$(\|\|O-)_4Al$	+ $(1/4)As_4$ + $(3/2)C_2H_6$	−4.0
3a	**R**	$(\|\|O-)_3AlMe + 4e^-$	+ OMe_2	+0.5
3b	**S**	$(\|\|O-)_4Al + \|\|O-Me + 6e^-$	+ OMe_2	−0.5
3c	**T**	$(\|\|O-)_4Al + \|\|O-Me$	+ $(1/2)As_4$ + OMe_2	−1.3
4−6a	**U**	$(\|\|O-)_2AlMe_2 + \|\|O-H + 2e^-$	+ $(1/2)C_2H_4$	+1.8
4b, 6b	**V**	$(\|\|O-)_3AlMe + 2\|\|O-H + 4e^-$	+ C_2H_4	+1.0
4c, 6c	**W**	$(\|\|O-)_4Al + 3\|\|O-H + 6e^-$	+ $(3/2)C_2H_4$	−1.1
(4)	**N**	$(\|\|O-)_4Al$	+ AsH_3 + $(3/2)C_2H_4$	−2.0
5b	**O**	$(\|\|O-)_3AlMe + 2e^-$	+ $(1/2)C_2H_4$ + CH_4	−0.8
5c	**P**	$(\|\|O-)_4Al + \|\|O-Me + 4e^-$	+ $(1/2)C_2H_4$ + CH_4	−1.0
5d	**Q**	$(\|\|O-)_4Al + \|\|As-Me + 2e^-$	+ $(1/2)C_2H_4$ + CH_4	−1.8
5e	**X**	$(\|\|O-)_4Al + \|\|O-H + 4e^-$	+ C_2H_4 + CH_4	−2.2
(5)	**N**	$(\|\|O-)_4Al$	+ $(1/4)As_4$ + $(3/4)C_2H_4$ + $(3/2)CH_4$	−4.2
6d	**R**	$(\|\|O-)_3AlMe + 4e^-$	+ C_2H_4 + H_2O	−0.6
6e	**Y**	$(\|\|O-)_4Al + \|\|O-H + 6e^-$	+ $(3/2)C_2H_4$ + H_2O	−2.3
6f	**Z**	$(\|\|O-)_4Al$	+ $(1/2)As_4$ + $(3/2)C_2H_4$ + H_2O	−3.1

[a] Models of surfaces after desorption **N**−**Z** are illustrated in Figure 7. Given values are in eV per $AlMe_3$ molecule reacting with As_2O_3 and relative to **A**.

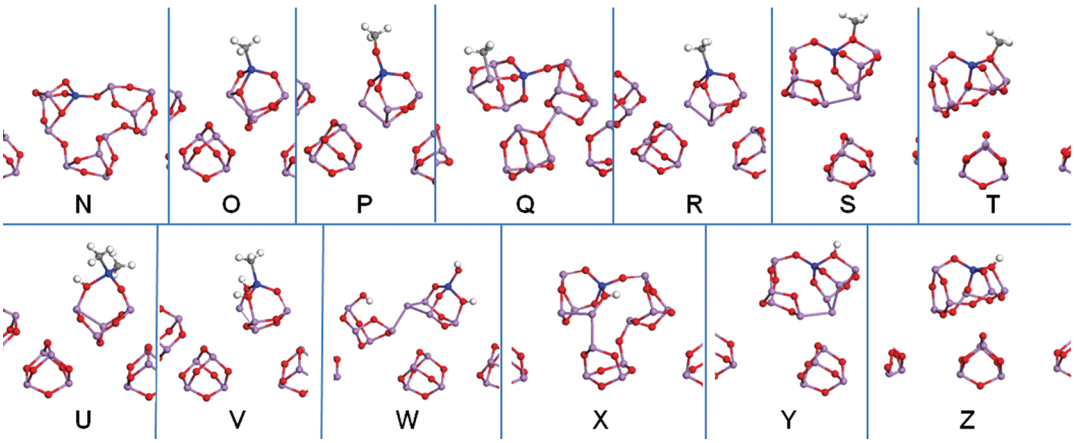

Figure 7. Surface models of products of desorption of volatile species: As_4, $AsMe_3$, AsH_3, CH_4, C_2H_4, C_2H_6, H_2O, and OMe_2 according to reactions 1−6 and their intermediates 2a−6f. Ball and stick representation: purple As, red O, blue Al, gray C, and white H.

reaction 2c: $\Delta G^{573K}_{(surf)} = -1.6$ eV relative to **A** (see Table 5). In reaction 2 one surface arsenic atom is reduced to elemental arsenic. This requires transferring three electrons (reaction 21). Therefore, from the product of reaction 2c we remove the remaining methyl group as Me^0 $[(1/2)C_2H_6]$:

$$Me^- \rightarrow Me^0 + e^- \quad (23)$$

thereby transferring one more electron to already-reduced As via reaction 19 in structure **Q**, transferring three electrons overall. Eliminating As^0 via reaction 21 from the surface [i.e., $(1/4)As_4$-(g)] and relaxing gives the final product **N** (Figure 7) along with an estimate of the energetics of surface reaction 2 (Table 5). The change in free energy computed according to the stoichiometry of reaction 2 is −4.0 eV per TMA.

OMe_2 may be formed from surface dissociation products **G**, **J**, **K**, where at least two methyl groups are oxidized. Desorption of OMe_2 according to reaction 3a gives product **R** (Figure 7) and is endothermic $\Delta G^{573K}_{(surf)} = +0.5$ eV relative to **A** (see Table 5). To estimate the energy for reaction 3, in accord with stoichiometry, it is necessary to oxidize three methyl groups via reaction 19 so two arsenics $[(1/2)As_4]$ are reduced via reaction 21. This procedure results in product **S**, with three As−As dimers, and a change in energy $\Delta G^{573K}_{(surf)} = -0.5$ eV relative to **A**. Desorption of OMe_2 and $(1/2)As_4$ leaves the surface product **T** and we can estimate the energy for reaction 3c: $\Delta G^{573K}_{(surf)} = -1.3$ eV.

dx.doi.org/10.1021/jp206566y |J. Phys. Chem. C 2012, 116, 643–654

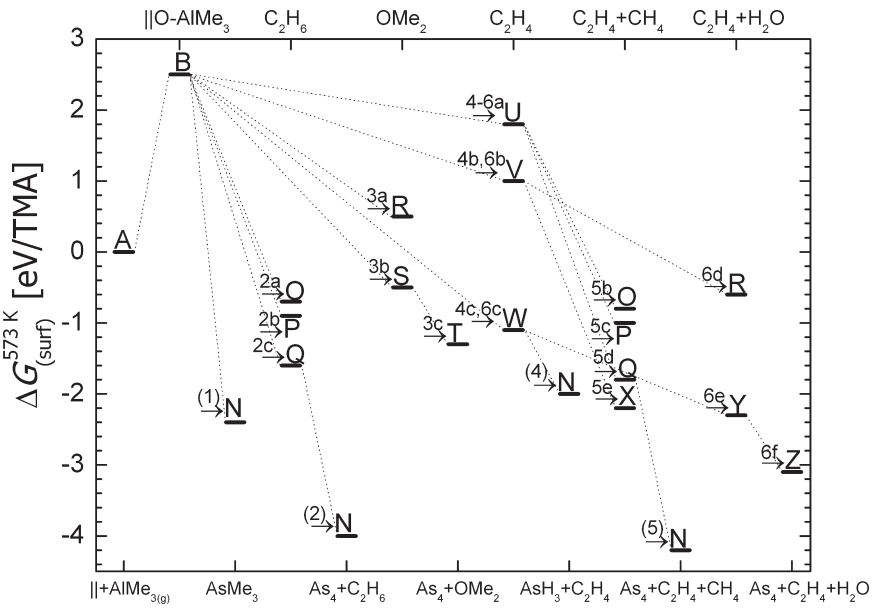

Figure 8. Potential free energy surface ($\Delta G^{573K}_{(surf)}$) showing minima for adsorption (B) and when volatile species are produced for surface reactions 1−6 and 2a−6f. The corresponding numerical values (in eV per $AlMe_3$ molecule reacting with As_2O_3 at 573 K) are shown in Table 5 with surface models shown in Figure 4, structures **A** and **B**, and Figure 7**N**−**Z**). Bottom and top *x* axes emphasize surface or gaseous products.

Surface energetics for the entire reaction 3 could not be calculated, since it produces fractional numbers of O atoms per TMA [$(3/2)OMe_2$].

Production of ethene in reactions 4 is shown to be strongly uphill. As mentioned before, there is probably a high barrier for the proton diffusion mechanism. The free energy computed for desorption of $(1/2)C_2H_4$ from structure **C** (Figure 4) via reaction 4a to form product **U** is $\Delta G^{573K}_{(surf)}$ = +1.8 eV (see Table 5, Figure 7). For surface reactions 4b the energy cost is a little less, $\Delta G^{573K}_{(surf)}$ = +1.0 eV, where C_2H_4 is formed from surface product shown in **F** (Figure 4) and leaves surface product **V** (Figure 7). Finally desorption of $(3/2)C_2H_4$ from structure **J** is exothermic in 4c surface reaction (Table 5). As a result of desorption of three-halves ethene, a hydroxylated arsenic oxide surface is produced, ||O−H, six electrons are transferred to surface arsenic (reaction 20), and as a consequence three As−As dimers are formed (product **W**, Figure 7). (On an oxidized GaAs surface, ||Ga−OH may also form, but this is beyond our current scope.) In the next reaction, desorption of three protons (H^+) from the hydroxyl groups and one reduced arsenic via reaction 22 gives the final gaseous product AsH_3 and surface product denoted as **W** (Figure 7). The Gibbs free energy for the entire reaction 4 modeled on the surface is $\Delta G^{573K}_{(surf)}$ = −2.0 eV (Table 5), making it the least favorable of the "clean-up" reactions that we have computed (Figure 8).

Reaction 5 is subdivided according to products: 5a, formation of $(1/2)C_2H_4$ (which is the same as 4a described above) and 5b−d, formation of CH_4 and arsenic reduction according to reaction 5. Structure **C** is the substrate for reactions 5b, 5c, and 5d, resulting in surfaces **N**, **O**, and **P**, respectively (Figure 7). In addition, elimination of C_2H_4 and CH_4 according to reaction 5e (Table 5) from structure **F** (Figure 4) leaves a partially hydroxylated surface for which the lowest energy structure that we have found is **T** (Figure 7). The fractional numbers of product molecules per TMA in reaction 5 seem to present a problem in calculating product desorption explicitly. However, eliminating fragments with the correct oxidation state results in proper stoichiometry. Thus, atoms are removed from the surface **Q** (||As−Me + $2e^-$) as As^0 + $CH_3{}^0$ (||As + Me^0 + $3e^-$), where $CH_3{}^0$ has C in the same overall oxidation state as the products $(1/4)C_2H_4$ + $(1/2)CH_4$. This procedure yields a surface free energy for the entire reaction 5: $\Delta G^{573K}_{(surf)}$ = −4.2 eV (Table 5). These surface energetics (Figure 8) confirm the bulk energetics already estimated in section 3.1 for the formation of C_2H_6 or C_2H_4 and CH_4 as a result of the "clean-up" effect.

Formation of C_2H_4 in reactions 6a−c (which are the same as 4a−c described above) are intermediates for reaction 6. Dehydration of the surface model **V** according to 2||O−H → ||−O−|| + H_2O(g), reaction 6d, will give the surface product **R**, Figure 7, and $\Delta G^{573K}_{(surf)}$ = −0.6 eV (Table 5). Dehydration of the surface model **W** according to reaction 6e is predicted to be thermodynamically more favored with $\Delta G^{573K}_{(surf)}$ = −2.3 eV (**V**, Figures 7 and 8). The surface energy for the entire reaction 6 also could not be calculated for the same reason as for reaction 3—the fractional number of O atoms in the final product [$(3/2)H_2O$]. Nevertheless, the partial data (reaction 6f, Table 5, surface product **Z**, Figure 7) place this process in the same energetic range as other redox mechanisms within this simple model and confirm our bulk estimate of the competition between reactions 2, 5, and 6 (Figure 8).

We have also computed adsorption of a second TMA molecule onto the hydroxylated surface **W**. The computed energies are the same as for the first TMA molecule adsorption ($\Delta G^{573K}_{(surf)}$/$\Delta E^{0K}_{(surf)}$ = +2.5/−0.7 eV, relative to **W**). This process can be also accompanied by CH_4 formation. In this reaction a proton may be transferred from one of the ||O−H groups to the C of the newly adsorbed $AlMe_3$ molecule, producing CH_4, which desorbs: ||O−H + ||O−$AlMe_3$ → (||O)$_2$−$AlMe_2$ + CH_4(g). This releases $\Delta E^{0K}_{(surf)}$ = −1.4 eV relative to **W**, but thermodynamically it is neutral: $\Delta G^{573K}_{(surf)}$ = 0.1 eV. This is close to the value computed by Elliott and Greer for the same reaction on an aluminum oxide substrate ($\Delta E^{0K}_{(surf)}$ = −1.2 eV).[19] In addition, we find that dehydration of the surface model **V**, according to reaction 6d, is less favored than methane production in reaction 5e. More importantly,

dx.doi.org/10.1021/jp206566y |*J. Phys. Chem. C* 2012, 116, 643–654

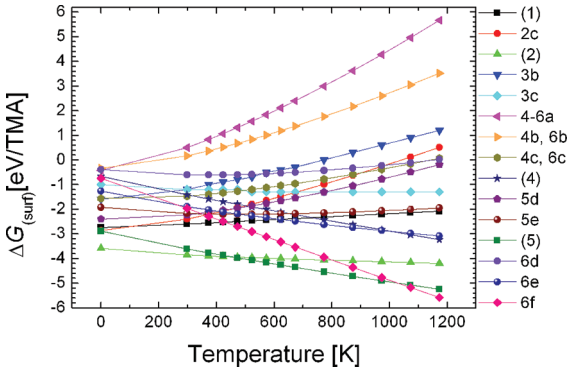

Figure 9. Temperature dependence of surface free energy for "clean-up" reactions 1−6 and their intermediates 2a−6f.

dehydration of the surface model **W** according to reaction 6e is predicted to be thermodynamically more favored than AsH_3 desorption. In all of these cases, surface protons are consumed via ||OH, ||Me, and/or incoming TMA to form CH_4 or H_2O. This suggests that reaction 4 is not only limited by electron transfer and accumulation, but also by proton concentration on the oxide surface, and this is governed by kinetics.

Figure 9 illustrates the effect of temperature on the candidate "clean-up" reactions in terms of the energy gained when products desorb. (The statistical likelihood and intercompetition between reactions is not shown, but is discussed in section 4.) Intermediates 4a−c leading to AsH_3 via reaction 4 are high in energy (also visible in Figure 8) and become progressively less favored with increasing temperature. Production of As_4 is consistently lower in energy (products **N** of reactions 2 and 5, and **Z** of reaction 6f also in Figure 8). Formation of OMe_2 along with As_4 is less favored than formation of other coproducts of As_4. At temperatures up to about 150 °C (423 K), the most energetically favored coproduct with As_4 is C_2H_6 (reaction 2), followed by C_2H_4 and CH_4 (reaction 5). $As_4 + C_2H_4$ and $As_4 + CH_4$ dominate in the range of 250−700 °C (523−973 K). At much higher temperatures (>800 °C), $As_4 + C_2H_4 + H_2O$ are the favored products (6f).

4. DISCUSSION

We have computed different mechanisms of decomposition of TMA on arsenic(III) oxide that can be responsible for the "clean-up" effect: methyl transfer, proton diffusion, methyl oxidation, and arsenic reduction. The possible surface intermediates are Al−Me_n, As−Me_n, O−Me, As−As, and Al−OH−As. As a result, the possible desorption products are As_4, $AsMe_3$, AsH_3, H_2O, CH_4, C_2H_6, C_2H_4, and/or OMe_2. The surface structures that we have generated (reaction intermediates) are linked together in order to reveal plausible reaction sequences. However, we have computed no actual pathways linking the structures (except where reactions occurred spontaneously during geometry optimizations, e.g., formation of As−As dimers). Transition state searches on a more realistic model of the oxidized surface would be needed for this, and the activation energies would give important information on the kinetics (albeit within the limited accuracy of DFT for activation energies). However, such a model would require a larger simulation cell and an improved description of van der Waals forces, which together would push the computational demands beyond current resources. In the absence of activation energies though, we can still discuss the overall shape of the potential energy surface formed by the minimum energy structures presented here.

Despite its limitations, the chosen surface model for As_2O_3 as part of an oxidized III−V substrate is able to reproduce energetics for reactions like TMA adsorption or CH_4 formation which are in very good agreement with the same reactions reported on an Al_2O_3 substrate.[19] Apparently, the molecular nature of arsenolite and its zero surface energy has a negligible effect on its reactivity with TMA, which is similar to that on other oxide surfaces. This suggests that TMA is a sufficiently strong combination of Lewis acidic Al and Lewis basic Me to adsorb and decompose on most oxide surfaces. Nevertheless we note that reconstructions of arsenolite are not accurate here because van der Waals forces are not taken into account. For this reason, we do not form any conclusions about the effect of multiple decomposition reactions in breaking As_4O_6 cages and replacing them with a surface film of Al_2O_3 and/or elemental As.

We assume that, on the hydroxylated native oxide surface, protons are primarily eliminated as CH_4, which does not affect As−O bonding and has little contribution to the "clean-up" effect. Other mechanisms like OH transfer are excluded by the high exothermicity of methane formation, i.e.,

$$AlMe_3(g) + \frac{3}{2}H_2O(g) \rightarrow \frac{1}{2}Al_2O_3(b) + 3CH_4(g), \quad \Delta G^{0K}_{(b)} = -5.9\ \text{eV} \tag{24}$$

$$AlMe_3(g) + H_2O(g) \rightarrow AlMe_2OH(g) + CH_4(g), \quad \Delta G^{0K}_{(b)} = -1.5\ \text{eV} \tag{25}$$

Therefore, as proposed before,[7,12,13] the driving force behind the "clean-up" mechanism is breaking As−O bonds and forming Al−O bonds. Since this transformation is achieved by all of the reactions 1−7 proposed here, it is reasonable that the calculations show them all to be exothermic. More surprisingly, we find that As−O bonds are also eliminated in a redox process when As−As dimers are formed, but this is not so energetically favorable. Therefore, we can propose alternative reagents (e.g., AsH_3) that should remove As_2O_3 without the formation of Al_2O_3, and this may be an interesting avenue for future experiments. Our calculations show that all the net bulk reactions are energetically downhill, and we conclude that these reactions might occur simultaneously on the oxidized III−V substrate.

Bulk and surface energetics agree in the overall trend for reactions 1−6. Both methods predict reactions 6, 5, and 2 to be almost equally exothermic around a typical ALD temperature range, then reaction 3 and 1, with the least favored being reaction 4, in that order up to $T \approx 750$ K. Above this temperature reaction 6 is more exothermic than reactions 5, 2, and 3; reaction 4 more favored than reaction 1 (see Figures 1 and 9).

Although reaction 7 was not modeled explicitly on the surface, it is clear to us that the various pathways responsible for partial carbon oxidation (surface reactions 2−6) may lead eventually to complete carbon oxidation in reaction 7 if there is enough reactant on the surface. Thermodynamics alone favor reaction 7, with products As_4, CO_2, and H_2O. However, we argue that the multiple steps involved in "clean-up" mean that thermodynamic products are not always accessible. Reaction 7 would need total decomposition of TMA and transfer of 24 electrons from C to As, as mentioned before. It is important to ask whether reactions 2, 3, 5, 6, and 7 will proceed without interruption until

12 electrons have accumulated in four surface arsenic atoms, allowing desorption as As_4. Some possible competing reactions are now discussed.

The energetics of ligand transfer favor ‖As−Me over ‖O−Me and over ‖As═CH_2 (section 3.4) and drive toward $AsMe_3$ (reaction 1). However, if O−Me does occur, we predict that it will combine with any neighboring ‖M−Me to give C_2H_6 (reaction 2), desorbing irreversibly and precluding the Me group from losing a proton and forming C_2H_4 (reactions 4−6). This leaves partially reduced As at the surface, which is also precluded from desorbing as $AsMe_3$. As shown in Figure 5, the statistics of ligand diffusion favor this outcome. Alternative side reactions 5 and 6, although energetically more favored, are statistically less likely, since these mechanisms require proton diffusion. Reactions 3 and 4 are both energetically and statistically less likely than reaction 2. Therefore, reaction 2 may indeed predominate to a sufficient extent that four TMA adsorptions on As_2O_3 yield a sequence of six desorbing C_2H_6 molecules, followed by desorption of one As_4 molecule.

On oxidized III−V substrates, however, there are more possibilities for consumption of partially reduced arsenic before desorbing as As_4. For instance, reduced arsenic may "getter" oxygen from gallium oxide on the surface, driven by the formation of GaAs:

$$\frac{1}{4}Ga_2O_3(b) + As^0(b) \rightarrow \frac{1}{2}GaAs(b) + \frac{1}{4}As_2O_3(b), \quad \Delta E^{0K}_{(b)} = +0.5\ eV \tag{26}$$

Adding this to reaction 2 we obtain

$$\frac{1}{4}As_2O_3(b) + \frac{1}{4}Ga_2O_3(b) + AlMe_3(g) \rightarrow \frac{1}{2}Al_2O_3(b) + \frac{1}{2}GaAs(b) + \frac{3}{2}C_2H_6(g), \quad \Delta G^{573K}_{(b)}/\Delta E^{0K}_{(b)} = -4.7/-4.9\ eV \tag{27}$$

which masks the fact that multiple partially reduced As atoms at the surface are involved in this overall reaction. A similar reaction may be written for In_2O_3 and InAs with computed $\Delta G^{573K}_{(surf)}/\Delta E^{0K}_{(surf)} = -4.8/-5.0$ eV. Reaction 27 illustrates that, on the oxidized III−V surface, GaAs or InAs are possible sinks for the III−V elements, rather than volatile molecules like As_4, AsH_3, $AsMe_3$, $GaMe_3$, and $InMe_3$.

The technological interest is in applying this reaction to the removal of all native oxides from III−V substrates prior to deposition of a high-*k* dielectric for an MOS structure. Therefore, having established the mechanism by which TMA achieves "clean-up" of As_2O_3, we now consider whether this works on other native oxides. The native oxides that have been detected on $In_{0.53}Ga_{0.47}As$ are As_2O_3, As_2O_5, Ga_2O_3, and In_2O_3.[8,13,31] The less stable form of arsenic oxide As_2O_5 is likely to be even more susceptible to reduction via reactions 2 than As_2O_3. By contrast, Ga_2O_3 and In_2O_3 are stable in oxidation state +3, and nonredox reaction 1 is the only likely candidate for TMA to directly "clean-up" these oxides:

$$\frac{1}{2}M_2O_3 + AlMe_3 \rightarrow \frac{1}{2}Al_2O_3 + MMe_3; \quad M = Ga, In \tag{28}$$

Calculated bulk energetics show that reaction 28 will take place: $\Delta G^{573K}_{(surf)}/\Delta E^{0K}_{(surf)} = -2.1/-2.4$ eV for M = Ga and $\Delta G^{573K}_{(surf)}/\Delta E^{0K}_{(surf)} = -2.1/-2.0$ eV for M = In. However, these energies are much smaller in magnitude than for M = As (see section 3.1, reaction 1), and this might explain why arsenic oxides are more effectively cleaned up than group III oxides by TMA.[7,8,12,13] An analogous reaction is proposed in the literature[50] by which SiO_2 is converted by TMA to $SiMe_4$ at temperatures above 600 K (325 °C), which is in that case supported by the relative formation energies of the oxides. We have recently proposed that the "clean-up" of Si_3N_4 by TMA may explain the substrate-enhanced ALD growth rate for Al_2O_3 on this substrate.[51] However, as shown above, indirect "clean-up" of gallium and indium oxides may also be possible via partially reduced arsenic at the surface, driven by the formation of GaAs and InAs (reactions 26 and 27).

On the basis of our results, we suggest the following reasons why TMA works well in "clean-up" of arsenic oxides. First, it is stable against autodecomposition in the gas phase (up to ca. 640 K[52−54]) and so is delivered to the surface intact. Second, it is a Lewis acid and adsorbs strongly onto oxide surfaces, ensuring an adequate lifetime on the surface for subsequent decomposition. Third, ligand transfer, driven by formation of Al−O, leads to a variety of decomposition pathways, which all produce solid Al_2O_3 and various gas-phase molecules containing C, H, and As. The anionic Me groups in TMA are reducing agents, and the thermodynamically predominant pathway for metalloid oxides is reduction, producing volatile molecules (e.g., As_4, reactions 2−6) or gettering oxygen from less reducible oxides (e.g., those of Ga, reaction 26). An alternative pathway is nonredox ligand exchange (reactions 1, 28), which allows nonreducible oxides (e.g., SiO_2) to be cleaned up; the key here is a strong bond between the ligand and the ion to be cleaned up.

We can therefore speculate why there are differences observed in performance of various precursors during initial exposure of III−V. For amide precursors ($Hf(NR_2)_4$, $Mg(NR_2)_2$; R = Me, Et), the anionic $[NR_2]^-$ ligand is susceptible not only to decomposition[55] but also to oxidation (in this case up to the +5 oxidation state is available for nitrogen) and therefore is a potential reducing agent toward metalloid oxides. By contrast, the chloride ligand is a very weak reducing agent and is unlikely to favor ligand exchange (relatively weak As−Cl bond), but as proposed before, "clean-up" with this ligand can be accounted for via an agglomeration reaction mechanism.[18] The observed difference in outcome when exposing III−Vs to $HfCl_4$ and $TiCl_4$ can be explained by the higher electropositivity of Hf. Hf would thus be more likely than Ti to scavenge oxygen from native oxides and show enhanced growth of its oxide. We conclude therefore that the performance of "clean-up" depends strongly on the electropositivity of the precursor metal, on the affinity of the precursor ligand to the oxide, and also on the chemical character of the oxide to be cleaned up.

5. CONCLUSION

In this work we have proposed ligand transfer and ligand transfer accompanied by charge transfer as the mechanism of removal of As−O bonds on an oxidized GaAs or InGaAs substrate in the very first pulse of TMA during ALD of Al_2O_3, a process known as "clean-up". From the computed thermodynamics (both in terms of potential energies and reaction statistics), we predict that the "clean-up" of III−V native oxides mostly produces As_4 gas, but also GaAs solid or InAs solid. Most C is predicted to form C_2H_6 (reaction 2) but with some C_2H_4, CH_4, and H_2O, and these products should be detectable during the TMA pulse. A wide variety of mechanisms are exothermic and therefore

competitive. In all cases, Al_2O_3 is formed in direct contact with the III−V substrate (e.g., Ga−O−Al linkages). We speculate that ‖As−Me will be the most abundant surface intermediate, as well as transient ‖As−As‖ and ‖O−Me that are markers for reactions 2−6, but we also note the necessity of assessing the kinetics of the proposed reactions in the future. As TMA exposure continues, "clean-up" of the native oxides will finish and the surface will become covered with species like ‖Al−Me, ‖Ga−Me, ‖In−Me, and ‖Al−Me_2, etc. We propose alternative reagents (e.g., AsH_3) that should remove As_2O_3 without the formation of Al_2O_3. "Clean-up" of an oxide film is shown to strongly depend on the electropositivity of the precursor metal, affinity of the precursor ligand to the oxide, and the redox character of the oxide. The predominant pathway for a metalloid oxide such as arsenic oxide is reduction, producing volatile molecules or gettering oxygen from less reducible oxides. An alternative pathway is nonredox ligand exchange, which allows nonreducible oxides to be cleaned up. This improved understanding of the chemical principles underlying "clean-up" allows us to rationalize and predict how other precursors perform the reaction.

AUTHOR INFORMATION

Corresponding Author

*Tel.: +353 21 490 4113. E-mail: sylwia.klejna@tyndall.ie.

ACKNOWLEDGMENT

This work was funded by Science Foundation Ireland under Grant No. 07/SRC/I1172 ("FORME", www.tyndall.ie/forme). The authors acknowledge the SFI/HEA Irish Centre for High-End Computing (ICHEC) for the provision of computational facilities and support. We are grateful to G. Hughes and B. Brennan of Dublin City University for helpful discussions.

REFERENCES

(1) George, S. M. *Chem. Rev.* **2009**, *110*, 111.
(2) Spicer, W. E.; Lindau, I.; Skeath, P.; Su, C. Y.; Chye, P. *Phys. Rev. Lett.* **1980**, *44*, 420.
(3) Hasegawa, H.; He, L.; Ohno, H.; Sawada, T.; Haga, T.; Abe, Y.; Takahashi, H. *J. Vac. Sci. Technol., B* **1987**, *5*, 1097.
(4) Spicer, W. E.; Liliental-Weber, Z.; Weber, E.; Newman, N.; Kendelewicz, T.; Cao, R.; McCants, C.; Mahowald, P.; Miyano, K.; Lindau, I. *J. Vac. Sci. Technol., B* **1988**, *6*, 1245.
(5) Ye, P. D. *J. Vac. Sci. Technol., A* **2008**, *26*, 697.
(6) Frank, M. M.; Wilk, G. D.; Starodub, D.; Gustafsson, T.; Garfunkel, E.; Chabal, Y. J.; Grazul, J.; Muller, D. A. *Appl. Phys. Lett.* **2005**, *86*, 152904.
(7) Milojevic, M.; Aguirre-Tostado, F. S.; Hinkle, C. L.; Kim, H. C.; Vogel, E. M.; Kim, J.; Wallace, R. M. *Appl. Phys. Lett.* **2008**, *93*, 202902.
(8) Hinkle, C. L.; Sonnet, A. M.; Vogel, E. M.; McDonnell, S.; Hughes, G. J.; Milojevic, M.; Lee, B.; Aguirre-Tostado, F. S.; Choi, K. J.; Kim, H. C.; Kim, J.; Wallace, R. M. *Appl. Phys. Lett.* **2008**, *92*, 071901.
(9) Hinkle, C. L.; Sonnet, A. M.; Vogel, E. M.; McDonnell, S.; Hughes, G. J.; Milojevic, M.; Lee, B.; Aguirre-Tostado, F. S.; Choi, K. J.; Kim, J.; Wallace, R. M. *Appl. Phys. Lett.* **2007**, *91*, 163512.
(10) Huang, M. L.; Chang, Y. C.; Chang, C. H.; Lee, Y. J.; Chang, P.; Kwo, J.; Wu, T. B.; Hong, M. *Appl. Phys. Lett.* **2005**, *87*, 252104.
(11) Chang, C. H.; Chiou, Y. K.; Chang, Y. C.; Lee, K. Y.; Lin, T. D.; Wu, T. B.; Hong, M.; Kwo, J. *Appl. Phys. Lett.* **2006**, *89*, 242911.
(12) Milojevic, M.; Hinkle, C. L.; Aguirre-Tostado, F. S.; Kim, H. C.; Vogel, E. M.; Kim, J.; Wallace, R. M. *Appl. Phys. Lett.* **2008**, *93*, 252905.
(13) Lee, H. D.; Feng, T.; Yu, L.; Mastrogiovanni, D.; Wan, A.; Gustafsson, T.; Garfunkel, E. *Appl. Phys. Lett.* **2009**, *94*, 222108.
(14) Tallarida, M. *Appl. Phys. Lett.* **2011**, *99*, 042906.
(15) Lin, L. *Appl. Phys. Lett.* **2011**, *98*, 082903.
(16) Granados-Alpizar, B.; Muscat, A. J. *Surf. Sci.* **2011**, *605*, 1243.
(17) Finnie, C. M.; Li, X.; Bohn, P. W. *J. Appl. Phys.* **1999**, *86*, 4997.
(18) Delabie, A.; Brunco, D. P.; Conard, T.; Favia, P.; Bender, H.; Franquet, A.; Sioncke, S.; Vandervorst, W.; Van Elshocht, S.; Heyns, M.; Meuris, M.; Kim, E.; McIntyre, P. C.; Saraswat, K. C.; LeBeau, J. M.; Cagnon, J.; Stemmer, S.; Tsai, W. *J. Electrochem. Soc.* **2008**, *155*, H937.
(19) Elliott, S. D.; Greer, J. C. *J. Mater. Chem.* **2004**, *14*, 3246.
(20) Perdew, J. P.; Chevary, J. A.; Vosko, S. H.; Jackson, K. A.; Pederson, M. R.; Singh, D. J.; Fiolhais, C. *Phys. Rev. B* **1992**, *46*, 6671.
(21) Kresse, G.; Furthmüller, J. *Phys. Rev. B* **1996**, *54*, 11169.
(22) Kresse, G.; Furthmüller, J. *Comput. Mater. Sci.* **1996**, *6*, 15.
(23) Vanderbilt, D. *Phys. Rev. B* **1990**, *41*, 7892.
(24) Kresse, G.; Hafner, J. *J. Phys.: Condens. Matter* **1994**, *6*, 8245.
(25) Ahlrichs, R.; Bär, M.; Häser, M.; Horn, H.; Kölmel, C. *Chem. Phys. Lett.* **1989**, *162*, 165.
(26) Perdew, J. P.; Burke, K.; Ernzerhof, M. *Phys. Rev. Lett.* **1996**, *77*, 3865.
(27) Eichkorn, K.; Treutler, O.; Öhm, H.; Häser, M.; Ahlrichs, R. *Chem. Phys. Lett.* **1995**, *242*, 652.
(28) Eichkorn, K.; Weigend, F.; Treutler, O.; Ahlrichs, R. *Theor. Chim. Acta* **1997**, *97*, 119.
(29) Schafer, A.; Horn, H.; Ahlrichs, R. *J. Chem. Phys.* **1992**, *97*, 2571.
(30) Wyckoff, R. W. G. *Crystal Structures*; Wiley Interscience: New York, 1963.
(31) Quagliano, L. G. *Appl. Surf. Sci.* **2000**, *153*, 240.
(32) Rojas-Lopez, M.; Gracia-Jimenez, J. M.; Vidal, M. A.; Navarro-Contreras, H. *J. Vac. Sci. Technol., B* **2001**, *19*, 622.
(33) Ballirano, P.; Maras, A. *Z. Kristallogr.—New Cryst. Struct.* **2002**, *217*, 177.
(34) Gibbs, G. V.; Wallace, A. F.; Cox, D. F.; Dove, P. M.; Downs, R. T.; Ross, N. L.; Rosso, K. M. *J. Phys. Chem. A* **2009**, *113*, 736.
(35) Tsuzuki, S.; Luthi, H. P. *J. Chem. Phys.* **2001**, *114*, 3949.
(36) Rydberg, H.; Dion, M.; Jacobson, N.; Schroumlder, E.; Hyldgaard, P.; Simak, S. I.; Langreth, D. C.; Lundqvist, B. I. *Phys. Rev. Lett.* **2003**, *91*, 126402.
(37) Jensen, J. O.; Gilliam, S. J.; Banerjee, A.; Zeroka, D.; Kirkby, S. J.; Merrow, C. N. *J. Mol. Struct.: THEOCHEM* **2003**, *664−665*, 145.
(38) Chrissanthopoulos, A.; Pouchan, C. *Vib. Spectrosc.* **2008**, *48*, 135.
(39) Reinhardt, F.; Richter, W.; Muller, A. B.; Gutsche, D.; Kurpas, P.; Ploska, K.; Rose, K. C.; Zorn, M. *J. Vac. Sci. Technol., B* **1993**, *11*, 1427.
(40) Cheng, C.-W.; Hennessy, J.; Antoniadis, D.; Fitzgerald, E. A. *Appl. Phys. Lett.* **2009**, *95*, 082106.
(41) Cho, A. Y. *Thin Solid Films* **1983**, *100*, 291.
(42) SpringThorpe, A. J.; Ingrey, S. J.; Emmerstorfer, B.; Mandeville, P.; Moore, W. T. *Appl. Phys. Lett.* **1987**, *50*, 77.
(43) Mizutani, T. *J. Vac. Sci. Technol., B* **1988**, *6*, 1671.
(44) Fiorentini, V.; Methfessel, M. *J. Phys.: Condens. Matter* **1996**, *8*, 6525.
(45) Ganduglia-Pirovano, M. V.; Sauer, J. *Phys. Rev. B* **2004**, *70*, 045422.
(46) Puurunen, R. L. *J. Appl. Phys.* **2005**, *97*, 121301.
(47) Tang, W.; Sanville, E.; Henkelman, G. *J. Phys.: Condens. Matter* **2009**, *21*, 084204.
(48) Sanville, E.; Kenny, S. D.; Smith, R.; Henkelman, G. *J. Comput. Chem.* **2007**, *28*, 899.
(49) Henkelman, G.; Arnaldsson, A.; Jónsson, H. *Comput. Mater. Sci.* **2006**, *36*, 354.
(50) Bartram, M. E.; Michalske, T. A.; Rogers, J. W. *J. Phys. Chem.* **1991**, *95*, 4453.
(51) Lamagna, L.; Wiemer, C.; Perego, M.; Spiga, S.; Rodríguez, J.; Coll, S.; Klejna, S.; Grillo, M.-E.; Elliott, S. D. Mechanisms for substrate-enhanced growth during the early stages of atomic layer deposition of alumina onto silicon nitride surfaces. *Chem. Mater.*, submitted **2011**.
(52) Puurunen, R. L.; Lindblad, M.; Root, A.; Krause, A. O. I. *Phys. Chem. Chem. Phys.* **2001**, *3*, 1093.
(53) Yeddanapalli, L. M.; Schubert, C. C. *J. Chem. Phys.* **1946**, *14*, 1.
(54) Lakomaa, E. L.; Root, A.; Suntola, T. *Appl. Surf. Sci.* **1996**, *107*, 107.
(55) Rodríguez-Reyes, J. C. *J. Appl. Phys.* **2008**, *104*, 084907.